LARGE-STROKE, FLEXURE-BASED

The design of a flexure-based suspension for a high-torque, iron-core direct-drive motor is presented. Over the full, large range of motion, the design provides the high radial stiffness (> 1,000 N/mm) required for resisting the high magnetic forces from the permanent magnets and iron core. Furthermore, it maintains a constant position of the pivot axis within 0.1 mm, to meet alignment tolerances. A prototype was realised and experimental validations have confirmed its high radial stiffness and applicability for iron-core torque motors.

MARK NAVES, MARIJN NIJENHUIS, WOUTER HAKVOORT AND DANNIS BROUWER

Introduction

In high-precision applications, flexure-based mechanisms are used for their deterministic behaviour due to the absence of play and friction. To maintain these deterministic properties, the actuators of flexure-based precision systems should also be free of play and friction. To this end, direct-drive actuators are often used as they do not rely on tribological contacts. Common Lorentz-type actuators, such as voice-coil, linear ironless or rotary ironless (torque) motors, rely on a permanent magnetic field and coil windings (without an iron core) to provide actuation forces.

The absence of an iron core means on the one hand that there is no disruptive cogging or high parasitic magnetic forces. On the other hand, this absence results in a reduced strength of the magnetic field and reduced thermal dissipation, which decreases the maximum actuation force. Therefore, ironless actuators are not always able to provide sufficient actuation force for demanding applications.

In contrast, Lorentz-type actuators with an iron core, in which the coils are mounted in an iron lamination stack, have actuation forces that are up to a factor of two larger, although at the expense of parasitic magnetic forces [1]. These parasitic forces are proportional to the misalignment between the magnet track and iron core away from the equilibrium position, which results in a destabilising negative stiffness.

To compensate for this negative stiffness, a stiff-bearing construction is required. This is often too demanding for flexure mechanisms, however, due to their limited support stiffness, especially when considering large-range-of-motion applications. Furthermore, large-stroke flexure mechanisms often suffer from a limited load capacity, insufficient for the resulting reaction forces on the bearing construction.

Additionally, the nonlinear nature of the elastic deformations of the flexures also results in parasitic motion that easily exceeds the alignment tolerances of typical actuators, because the air gap between the magnet track and coil is often small. Lastly, due to the negative stiffness provided by the iron core, parasitic motion results in additional parasitic pull-in forces.

This article presents a flexure-based rotary actuator suspension with 60° range of motion. This actuator suspension was designed for use in a flexure-based, large-range-of-motion hexapod system (the T-Flex [2], videos in [3]) for which high actuator torque is required (up to 40 Nm).

Actuator

The direct-drive motor considered is an iron-core, permanent-magnet motor (Tecnotion's QTR-A-133-60), which allows for an ultimate torque of 55.5 Nm. The negative radial stiffness resulting from the iron core and permanent magnets is approximately 350 N/mm, while a radial alignment of < 1 mm is required to prevent contact between the rotor and stator. A schematic drawing with the main dimensions of the actuator is provided in Figure 1.

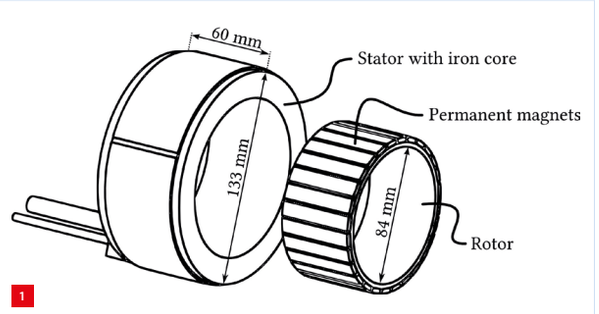

Exploded view of the QTR-A-133-60 torque motor with the main dimensions.

AUTHORS' NOTE

Mark Naves and Marijn Nijenhuis (both Ph.D. students), Wouter Hakvoort (assistant professor) and Dannis Brouwer (professor) are all members of the chair of Precision Engineering in the Department of Mechanics of Solids, Surfaces & Systems at the University of Twente (NL).

m.naves@utwente.nl
www.utwente.nl/en/et/ms3/research-chairs/pe

Flexure-based suspension

For commonly used flexure joints for a single rotational degree of freedom (DoF), such as the cross-spring pivot consisting of two (or more) separate leafsprings, the motion of the shuttle (in this case attached to the rotor) is typically approximated by a circular motion around a fixed axis of rotation. However, for larger deflection angles, the motion path of the shuttle deviates from this circular path, due to the non-linear nature of the elastic deformations of the flexures. For the considered range of motion of 60° (–30° to +30°), this deviation easily exceeds the required alignment tolerance of 1 mm between rotor and stator.

In order to minimise the parasitic motion of the rotor, the butterfly flexure hinge design was selected, as it is known for its small parasitic motion due to the smart compounding of the leafsprings [3]. This hinge effectively consists of a stacked arrangement of four cross-spring pivots with coinciding rotation axis, schematically illustrated in Figure 2. For this joint, the parasitic motion of the first and fourth cross-spring pivots is compensated for by the opposed parasitic motion of the second and third cross-spring pivots. Therefore, the parasitic motion is strongly reduced and its magnitude can be approximated by [4]:

$$d_{par} = \left(\frac{1}{cos(\alpha_2)} - \frac{1}{\cos(\alpha_1)}\right)\frac{9\lambda^2 - 9\lambda + 1}{120} L\theta^2$$

Here, $\lambda > 1$ in order to prevent interference between the individual cross-spring pivots in the stacked arrangement and α provides the angle between the individual leafsprings. Please note that this equation only provides the kinematic parasitic motion of the butterfly hinge, disregarding (magnetic) reaction forces on the system that will cause additional displacement. Considering a realistic value of $\lambda = 1.1$ combined with $\alpha_1 = 35°$ and $\alpha_2 = 55°$ and a range

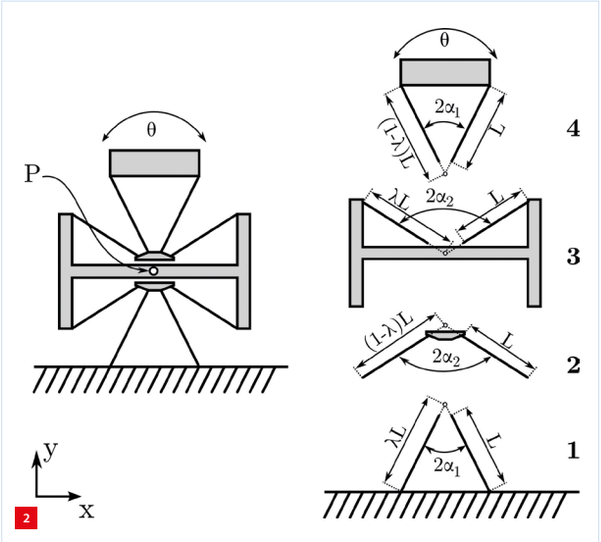

Schematic overview of the butterfly hinge with the rotation axis provided by P.

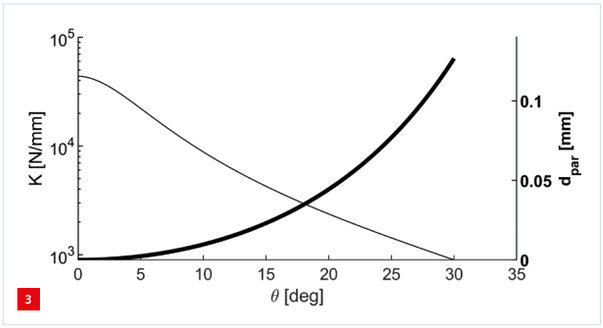

Support stiffness (K) and parasitic motion (d_{par}) of the optimised butterfly hinge.

of motion of $\theta = 30°$, this results in a parasitic motion of $L/341$ [m], which is well below 1 mm for typical values for L.

For the design of the butterfly hinge, the width of the joint (the z-dimension in Figure 2) was fixed to 100 mm and the length (L) and thickness (t) of the flexures were optimised to maximise support stiffness in the most compliant direction (considering the full range of motion). For the optimisation, the flexible-multi-body package Spacar [5] was used, combined with an adapted Nelder Mead-based shape-optimisation algorithm [6]. As for material, tool steel (Stavax) was selected, with the allowable stress limited to 600 MPa, which is about 40% of the yield stress of the material.

The resulting support stiffness and parasitic motion of the optimised butterfly hinge (L = 35 mm and t = 0.33 mm), including the negative stiffness induced by the rotor magnets, is provided in Figure 3. At the maximum deflection angle of $\theta = 30°$, a radial support stiffness (K) of almost 1,000 N/mm (–350 N/mm negative stiffness included) was obtained, combined with a parasitic deflection of 0.12 mm, which is well below the allowed 1 mm.

For the butterfly hinge, it has to be noted that each intermediate body between each set of flexures has an unintended rotational DoF around the rotation axis of the joint, introducing three unconstrained DoFs. For most flexure-based mechanisms, underconstrained intermediate bodies dramatically deteriorate support stiffness (especially for large deflection angles) due to the coupling between external loads applied to the end-effector and the unconstrained DoFs of the intermediate bodies, similar to the compounded parallel leafspring guidance without slaving mechanism [7]. However, as the instant centre of rotation of each intermediate body and the end-effector coincide and hardly vary, external loads on the end-effector do not result in a reaction moment in the DoFs of the intermediate body.

With respect to the dynamic behaviour of the joint, however, the unconstrained intermediate bodies can result

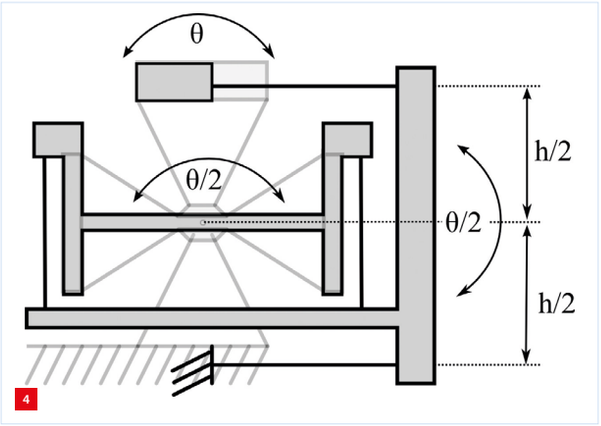

Schematic overview of a butterfly hinge with slaving mechanism.

in unwanted vibrations of the system. The two small intermediate bodies positioned between the first and second set of leafsprings and the third and fourth set of leafsprings have a high natural frequency in the unconstrained DoF, due to the low inertia with respect to the rotation axis of the joint.

Therefore, these unconstrained DoFs typically do not introduce unwanted vibrations in the frequency range of interest. The large intermediate body positioned between the second and third flexure set does potentially lead to unwanted vibrations due to its large size and high inertia.

In order to eliminate this underconstraint, an additional slaving mechanism can be added that couples the motion of the end-effector and the intermediate body with a ratio of two-to-one [3]. A schematic overview of a butterfly hinge with slaving mechanism is provided in Figure 4.

Prototype design

Based on the optimisation results, a prototype of the flexible actuator suspension for the selected torque motor was constructed. An exploded view of the prototype is provided in Figure 5, which shows the suspension for two actuators with parallel rotation axes.

In the design, two butterfly hinges (1) with a width of 50 mm and a slaving mechanism (2) are placed on either side of an aluminium rotor hub (3) that carries the rotor (4). The central 'large' intermediate bodies (5) that are slaved by the slaving mechanisms are interconnected with an aluminium body (6). This body is placed inside the rotor hub and provides a stiff connection between the intermediate slaved bodies.

Furthermore, a linear encoder (7) is placed on the rotor hub (concentric with the rotor) to provide sensing of the rotor position, and a mechanical stop (8) and optical switch (9) are added to prevent excessive rotation of the rotor. The stationary part of the actuator containing the coils, the stator (10), is fixed

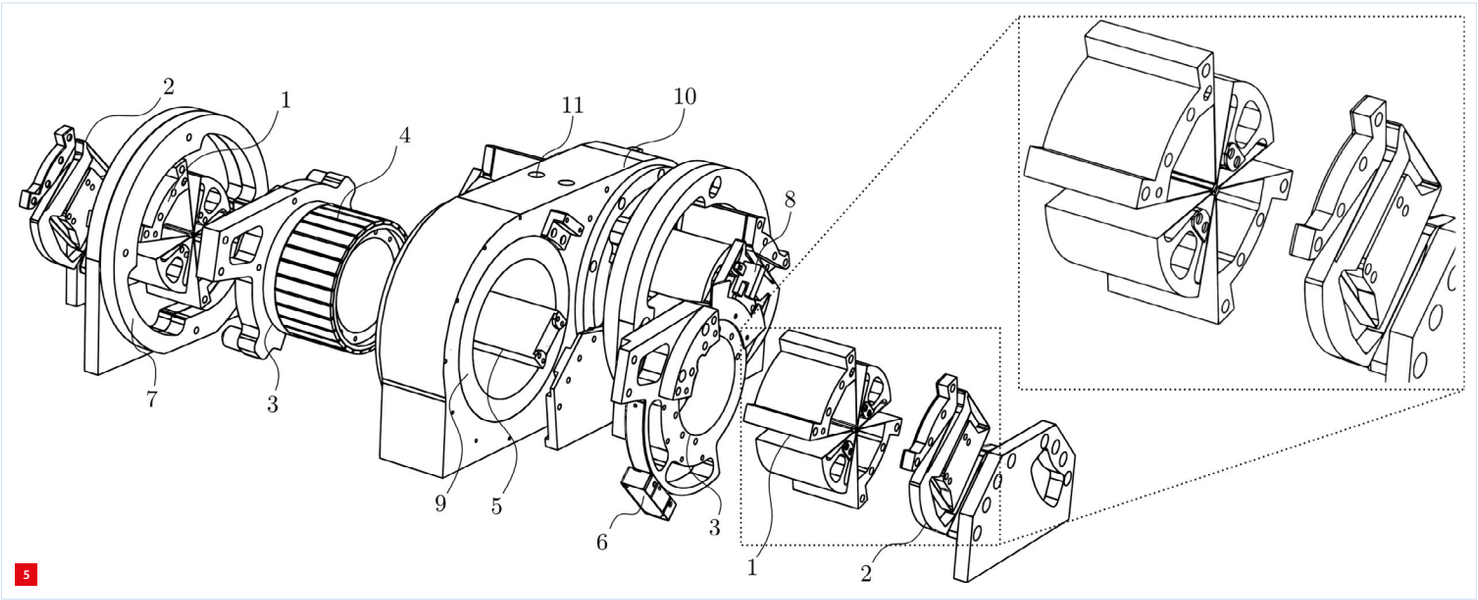

Two actuator suspensions with parallel rotation axis (front actuator suspension in exploded view).
1) Butterfly hinge.
2) Slaving mechanism.
3) Rotor hub connected to both butterfly hinges.
4) Permanent magnets of the rotor.
5) Body coupling intermediate bodies of both butterfly hinges.
6) Encoder.
7) Mechanical stop.
8) Optical switch.
9) Actuator's stator.
10) Stator housing.
11) Cooling channels.

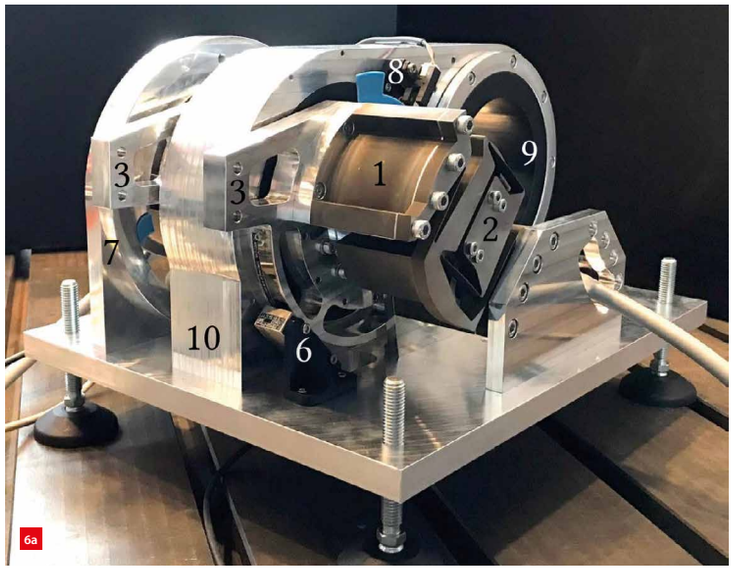

6a

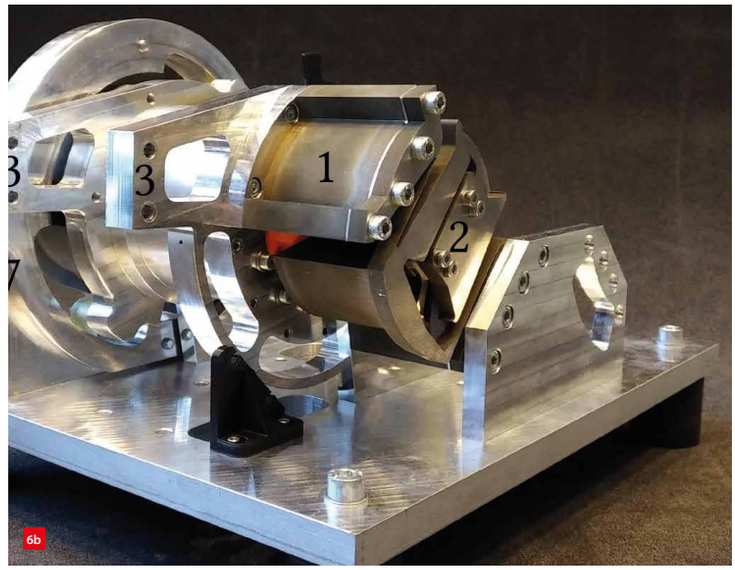

6b

The assembled flexure-based actuator suspension, with 1) butterfly hinge, 2) slaving mechanism, 3) rotor hub, 6) encoder, 7) mechanical stop, 9) actuator's stator, and 10) stator housing.
(a) Overview.
(b) Trimmed view, with the torque motor and stator housing removed.

inside an aluminium frame (11). This frame holds the stator and improves the thermal dissipation for the actuator. Furthermore, the housing is equipped with cooling channels (12) to actively cool the stator for high-load applications.

An overview of the realised prototype is provided in Figure 6 and the video [V1] demonstrates the low hysteresis of the flexure-based design. It has to be noted that insertion of the rotor during assembly requires special attention and additional assembly tools to provide resistance to the negative radial stiffness and to ensure good alignment between the stator and rotor.

As two butterfly hinges at each side of the rotor are used for supporting the actuator, the system is overconstrained, which could result in excessive stress or increased stiffness in the DoF or even decreased stiffness in the support directions. Therefore, care was taken in the positioning of the two individual butterfly hinges to ensure good alignment between them. In particular, the locations of the rotation axis of both butterfly hinges require good alignment, which is ensured by using dowel pins for both hinges.

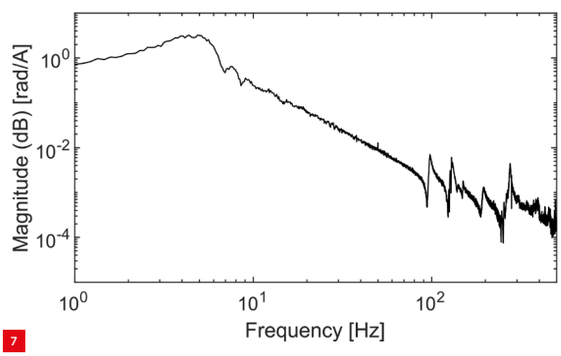

7

Transfer function from current (A) to rotor position (rad) at θ = 25°, with the first parasitic eigenfrequency at 98 Hz.

Experimental validation

Support stiffness

To validate the support stiffness of the rotor suspension, the frequency of the first parasitic vibration mode of the end-effector was evaluated, which is directly related to the (critical) radial support stiffness. This parasitic vibration mode consists of a translational radial motion approximately parallel to the encoder head on the rotor hub, which can be sensed by the encoder.

To determine the stiffness, the frequency response from actuator current to rotation of the rotor was evaluated, which is provided in Figure 7. This frequency response was evaluated as close to the maximum deflection angle as possible while still allowing for sufficient range of motion for a sweep signal on the input current. From this data, the first (damped) eigenfrequency in the DoF of the system could be observed at about 5 Hz. At 98 Hz, the first parasitic eigenfrequency could be observed, which can be related to the off-axis support stiffness of the system.

In combination with the 3.0 kg mass of the end-effector, consisting of the rotor, rotor hub and a part of the butterfly hinges, this 98 Hz eigenfrequency provides a radial support stiffness of approximately 1,138 N/mm. This is in good agreement with simulations and confirms the intended high radial stiffness of the butterfly hinges (simulated value $K \approx 1{,}400$ N/mm at $\theta = 25°$, Figure 8). The slightly lower stiffness values in the measurement can be related to additional (i.e. non-zero) compliance of the frame parts, which was disregarded in the simulations.

Repeatability

As the system is free of play and friction (and therefore free of self-locking and limit cycling), its repeatability is directly determined by its stand-still performance. To test the repeatability, a representative load was attached to the rotor (a solid block of aluminium resulting in a total inertia of 0.066 kgm²) and the rotor was moved to a setpoint while the positioning error was tracked. For the presented case, the rotor was moved from $\theta = -22.5°$ to $\theta = -2.5°$ in 0.2 s. The resulting error for a single movement is provided in Figure 8a, where motion starts at $t = 0$ s. Furthermore, a more detailed view of the position of the rotor between $t = 2$ s and $t = 2.5$ s is provided in Figure 8b.

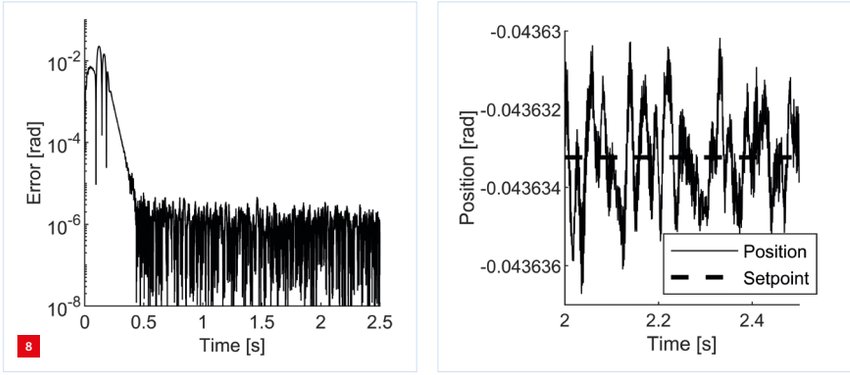

Position error for tracking a reference signal moving from θ = –22.5° (t = 0 s) to θ = –2.5° (t = 0.2 s).

From the results it can be observed that the position of the rotor has converged to the target position in about 0.5 s, after which it fluctuated around the target position with an average error of 1.1 µrad rms. These fluctuations in the position are caused by current fluctuations (current ripple) from the motor driver (±5 mA rms noise), resulting in deviations in the generated torque (motor constant 5.57 Nm/A).

As stated earlier, due to the absence of friction, no stick-slip behaviour is present in the flexure-based bearing suspension, resulting in no (mechanical) resistance to small current (torque) variations. Therefore, small fluctuations in the provided current directly cause rotor positioning errors that produce a vibrating motion around the reference position. The driver can be identified as the source of this error as these fluctuations are only present when the motor driver is active.

Stand-still performance can be improved by either reducing the noise output of the driver (dedicated electronics) or by reducing the sensitivity of the rotor position with respect to current fluctuations. The latter can be achieved by reducing the motor constant (i.e. selecting a different actuator) or by increasing the inertia of the system. However, this comes at the expensive of the maximum acceleration that can be achieved and does not affect the ratio between acceleration and stand-still performance.

Conclusion

A large-range-of-motion, flexure-based suspension for an iron-core, direct-drive torque motor with high power density has been designed. The system allows for 60° range of motion combined with an ultimate torque of 55 Nm, featuring high repeatability. The repeatability was measured at 1 µrad rms positioning error with a load of 0.066 kgm², at present restricted by current noise of the motor driver.

For the actuator suspension, a butterfly hinge has been modified and optimised to result in only 0.1 mm parasitic radial displacement over the range of motion, which limits pull-in forces typical for iron-core actuators. The radial support stiffness exceeds 1,000 N/mm. This provides adequate support stiffness to compensate for the negative stiffness induced by the iron core of the actuator.

Experimental validations have confirmed the support stiffness and proven the applicability of a flexure-based suspension for high-power-density, iron-core actuators.

REFERENCES

[1] Laithwaite, E.R., and Nasar, S.A., "Linear-motion electrical machines", *Proc. IEEE*, 58(4), pp. 531-541, 1970.
[2] Naves, M, Aarts, R.G.K.M., and Brouwer, D.M., "Maintaining high support stiffness – Large-stroke spherical flexure joint", *Mikroniek*, 59 (3), pp. 17-21, 2019.
[3] *www.utwente.nl/en/et/ms3/research-chairs/pe/T-Flex*
[3] Henien, S., "Short Communication: Flexure delicacies", *Mechanical Sciences*, 3, pp. 1-4, 2012.
[4] Hongzhe, Z., and Shusheng, B, "Accuracy characteristics of the generalized cross-spring pivot", *Mechanism and Machine Theory*, 45(10), pp. 1434-1448, 2010.
[5] Jonker, J.B., and Meijaard, J.P., "Spacar – computer program for dynamic analysis of flexible spatial mechanisms and manipulators", pp. 123-143 in Schiehlen, W. (ed.), *Multibody Systems Handbook*, Springer-Verlag, Heidelberg, 1990.
[6] Nelder, J. A., and Mead, R., "A Simplex Method for Function Minimization", *Computer Journal*, 7(4), pp. 308–313, 1965.
[7] Jones, R.V., "Some uses of elasticity in instrument design", *Journal of Scientific Instruments*, 39(5), pp. 193-203, 1962.

VIDEO

[V1] Fully flexure-based motor suspension
www.youtube.com/watch?time_continue=4&v=rzQorFtXK3I&feature=emb_logo